


Article

Experimental Study on Shear Strengthening of RC Beams with an FRP Grid-PCM Reinforcement Layer

Rui Guo ^{1,2,3,*} , Lianheng Cai ¹, Shinichi Hino ³ and Bo Wang ^{4,*}

¹ Department of Building Engineering, School of Civil Engineering, Southwest Jiaotong University, Chengdu 610031, China

² Key Laboratory of Seismic Engineering of Sichuan Province, Southwest Jiaotong University, Chengdu 610031, China

³ Department of Civil Engineering, Kyushu University, 744, Motoooka, Nishi-ku, Fukuoka 8190395, Japan

⁴ School of Civil Engineering, Chang'an University, Xi'an 710061, China

* Correspondence: guor4867@swjtu.edu.cn (R.G.); chnwangbo@chd.edu.cn (B.W.);
Tel.: +86-028-8776-7556 (R.G.)

Received: 17 June 2019; Accepted: 22 July 2019; Published: 25 July 2019



Abstract: This paper investigates the shear strengthening effect of a number of reinforced concrete (RC) beams strengthened by a reinforcement layer which combines carbon fiber reinforced polymer (CFRP) grid and polymer cement mortar (PCM). A total of ten RC beams, including three types of specimens as Series A and seven kinds of specimens as Series B, were prepared and investigated. The test variables in both series of experiments included various reinforcement ranges and different reinforcement amounts that consisted of CFRP grids' spacing and cross-section areas. The experimental results suggest that the shear strengthening effect of the CFRP grid-PCM layer for RC beams is obvious and adequate. Meanwhile, better performance is observed if the CFRP grid-PCM reinforcement layer is used for the full sectional reinforcement of RC beams with an I-shaped profile, in contrast to RC beams with reinforcement of the web only. In addition, a new evaluation method based on the effective strain of the CFRP grid is developed to determine the shear capacity of RC beams strengthened by a CFRP grid-PCM layer.

Keywords: fiber reinforced polymer (FRP) grid; polymer cement mortar (PCM); shear strengthening; reinforced concrete (RC) beams; evaluation method

1. Introduction

Over the last two decades, there has been a great demand for the strengthening or retrofitting of existing reinforced concrete (RC) structures due to ageing, the increment of the service load, the fact that they were designed using former guidelines, or even due to earthquakes. For example, a large number of concrete structures designed and constructed according to former standards had collapsed or were damaged in the Great East Japan Earthquake in 2011. At that time, a sluice with an I-shaped profile (Figure 1), placed across a river embankment to drain wastewater and pump water from the river, was damaged due to the occurrence of uneven settlement. Moreover, it has been found that the steel reinforcement ratio of existing concrete structures designed using the former standard was inadequate. For this reason, a certain strengthening method is required to make sure the capacity of sluice is sufficient in shear. If using reinforced concrete to enlarge the cross section, the inhibition rate of the cross section becomes too large and a thicker concrete covering should be applied to prevent corrosion of steel bars. As a result, this method may have an adverse impact on the normal use of sluice, so another method should be used to instead of enlargement of the cross section.

Some strengthening and retrofitting materials have been developed for existing concrete structures in the last decade, including textile reinforced mortar (TRM) [1–6], fiber reinforced cementitious matrix (FRCM) [7–12], textile reinforced concrete (TRC) [13–16], steel-reinforced grout (SRG) [17,18], and fiber reinforced polymer (FRP) composites [19–25]. Among them, fiber reinforced polymer (FRP) composites, including FRP sheets, FRP plates, FRP grids, and so forth, have been demonstrated to be an effective solution due to their favorable and prominent properties (e.g., light weight, high tensile strength, excellent corrosion resistance, and durability in harsh environments) [26,27]. FRP grids (Figure 2), a kind of FRP composite that has been proposed in the past decade, are made of high-strength fibers such as carbon fibers impregnated with a suitable resin system to form a grid pattern, and the main difference between FRP grids and FRP sheets/plates include the production process, cross section, and stiffness. Currently, numerous experimental studies have been performed on RC beams strengthened with externally bonded FRP sheets/plates, but those were always conducted together with epoxy-based materials used as bonding agent. Thus, the strengthening effect in flexural or in shear largely depends on these organic systems (usually an epoxy system) at the bonding interface between FRP sheets/plates and the concrete substrate. However, the epoxy-based materials have their own weaknesses, which primarily include the poor fire resistance, easy degradation under strong UV radiation, and low efficiency in both over-high/low temperature and moisture environments [28–30]. These disadvantages have partially compromised the attractive properties of strengthening techniques mentioned before in some engineering applications. For these reasons, the bonding behavior at the interface may deteriorate rapidly if existing concrete structures lie in harsh environments, such as over-high/low temperature, in the presence of moisture, or even near fire and underwater.

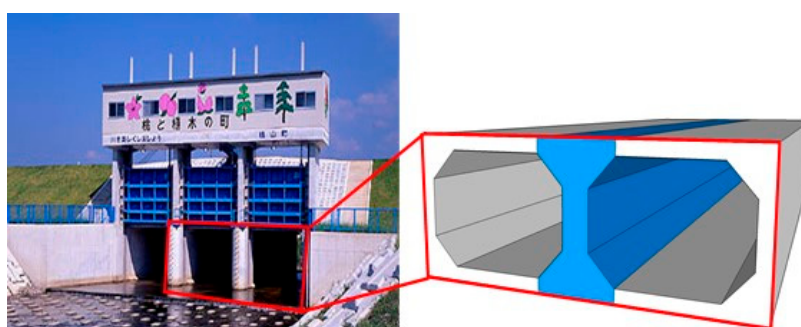


Figure 1. Sluice.

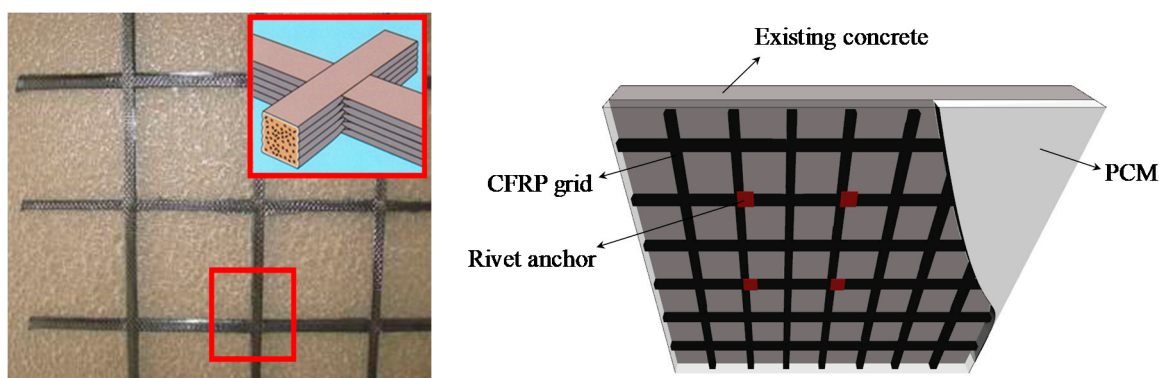


Figure 2. Carbon fiber reinforced polymer (CFRP) grid and schematic illustration of the strengthening method.

Therefore, some scholars have suggested replacing the epoxy systems with some inorganic cementitious materials to develop two major strengthening systems which combine FRP composites and cement-based materials [31], namely FRP sheets/plates bonded with a cementitious material [32] and FRP grids bonded with cement mortar [33,34]. Compared to the former strengthening method,

the advantages of FRP grids bonded with a cement-based material are summarized as follows: (a) the stress transfer between the FRP grid and cementitious materials is more efficient, caused by the improving of the impregnation [32,35]; (b) the drawbacks observed with the FRP sheets/plates with respect to uneven pasting and empty drums can be effectively avoided, especially when the strengthening areas are excessively large; and (c) for FRP grid strengthening, the rivets are usually considered to be a temporary anchor to attach the FRP grid on the external surface of concrete beams such that better bonding at the interface may be obtained to some extent.

As mentioned before, FRP grids are usually fixed and bonded to concrete by spraying or laminating a thin covering of normal mortar. However, normal mortar is easily broken due to its properties of low tensile strength and brittleness. Thus, several cementitious materials used as a thin strengthening layer, such as engineered cementitious composite (ECC) matrix [33,34,36] and polymer cement mortar (PCM) [37–39], have been proposed by scholars from all over the world to take the place of normal mortar with low strength. PCM, a new inorganic material used in strengthening fields, is made by pouring a small volume of organic polymer (e.g., acrylic copolymer [40], arene-perfluoroarene [41,42]) into a kind of cement mortar. The purpose of this is to improve the performance of the original inorganic materials, as it displays such properties as high tensile strength, superior corrosion and seepage resistance, lower incidence of dry cracking, as well as better bonding performance between PCM and the original concrete substrate [37,43,44].

A large number of relative studies on various FRP composites in shear strengthening have been discussed in recent years. For example, Liu et al. and Koutas et al. [6,45,46] demonstrated the current state of research regarding RC members retrofitted by CFRP grid-PCM layer, indicating that regardless of the flexural or shear reinforcement effect, the load-carrying capacity of RC members retrofitted by CFRP grid-PCM was adequate. Teng et al. [47] summarized the development and application of new structural materials, such as FRP composites, showing that the load capacity and ductility of strengthened structures were increased compared to unreinforced structures. Chen et al. [48] and Lu et al. [49] considered that the debonding failure of FRP composites with various formations (e.g., FRP grids/sheets) usually appeared on the concrete surface prior to concrete crushing during the shear resistance process. Zheng et al. [50] conducted several shear tests with RC beams externally bonded with FRP grid and UHTCC. The results showed that the shear strengthening effect produced by this method was very good, and studied the shear-compression failure and partial debonding of FRP grids regarding the ultimate state for these beam specimens with different reinforcement ratios. Ding et al. [51] assessed the strengthening effect by comparing FRP grids and FRP sheets, indicating that the load-carrying ability and safety of beams reinforced with FRP grids were better than FRP sheets. In addition, Spadea et al. [52] and Ferreira et al. [53] noted that the structural effectiveness of FRP composites in strengthening RC members was quite important to predict the load capacity of the strengthened beams. Therefore, previous investigators have pointed out that the evaluation method, which determines the contribution of the FRP composites for RC beams in shear, should carefully consider the effective strain of the FRP composites [54–57]. However, existing calculated methods in shear are not suitable for the FRP grid because its stress transfer mechanism is different from traditional FRP composites (e.g., FRP sheets, FRP plates, and FRP bars). Moreover, at present, few studies have explored the reinforcement range and reinforcement amount of I-shaped RC beams, especially those strengthened by FRP grids.

Taking the above background into consideration, this paper aims to explore the shear strengthening effect of RC beams with I-shaped profiles using FRP grid-PCM reinforcement layer. For this purpose, a total of ten beam specimens are divided into two series (called Series A and Series B later) and are introduced in different sections. Initially, three kinds of specimens (Series A) under various reinforcement ranges are used to investigate which type is the most suitable for RC beams with I-shaped profiles; then, based on the research results of Series A, the other series, Series B, are investigated in order to explore the shear resistance effect on concrete beams under different reinforcement amounts. The load–deflection responses, load–strain responses, and crack patterns are compared among all

specimens. Moreover, a new evaluation method for the shear capacity of RC beams with a combination of CFRP grid and PCM as a reinforcement layer, which is based on the effective strain of the CFRP grid, is subsequently developed.

2. Experimental Study on Reinforcement Range

2.1. Test Programme

There are three types of specimens with different CFRP grid-PCM reinforcement ranges in Series A, including the control beam N0 with no reinforcement, and the specimen RWC5 that is reinforced by a CFRP grid of CR5 type on the web only, while the remaining RHWC5 is similar to RWC5 but the reinforcement range covers both the web and the haunch, as indicated in Table 1.

Table 1. Details of the beam specimens of Series A.

Type	Existing Sample		Reinforcement Portion	Reinforcement Range	Thickness of PCM, mm
	Stirrups, mm	Tensile Steel Bars, mm	CFRP Grid (Spacing: Vertical × Horizontal), mm		
N0			-	-	-
RWC5	HRB335 D10@250	HRB335 D32 × 4	CR5 (150 × 50)	Web	15
RHWC5				Haunch + Web	15

Note: (1) RWC5 means reinforcement in web with a CFRP grid of type CR5, and RHWC5 means reinforcement in haunch and web with a CFRP grid of type CR5; (2) the FRP grid is embedded in PCM with a thickness of 15 mm at each side. (3) HRB-X means the strength class of steel bars; D-X means the steel bar with a diameter of X mm; @-X means the interval of stirrups is X mm.

Figure 3 shows the manufacturing process for the specimens. Initially, concrete beams with an I-shaped profile were produced and then cured for 28 days. Subsequently, original beams were polished by vacuum blasting for surface treatment before the CFRP grid was attached to the lateral surface of the concrete beam, with rivets used as temporary anchorage. Finally, in order to avoid the occurrence of dehydration phenomenon, primer mortar was sprayed or painted prior to PCM shotcrete.

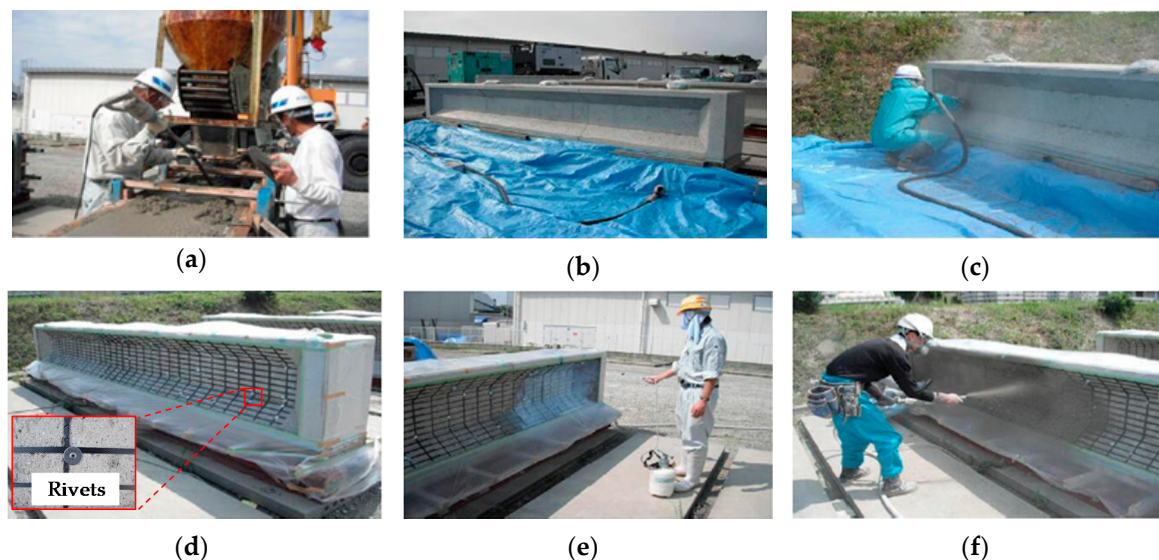


Figure 3. The manufacture process of specimens: (a) Concrete cast; (b) Original concrete beam; (c) Vacuum blast; (d) CFRP grid installation; (e) Primer mortar spray; (f) PCM shotcrete.

Grade HRB 335 steel bars with a diameter of 10 mm and spaced at an interval of 250 mm were used as stirrups, where the calculated stirrup reinforcement ratio was 0.38%. The compressive and tensile steel bars of Grade HRB 335 with a diameter of 32 mm were placed in the upper and bottom

region to resist the compressive and tensile force, respectively. The tensile steel reinforcement ratio calculated in this series (i.e., Series A) was 4.48%, the purpose of which is to ensure a higher flexural capacity than shear capacity, resulting in the typical shear failure prior to flexural failure in the end. Further, the shear span ratio of 2.75 in all specimens, which meets the demand of GB 50010-2010 [58], guarantees the occurrence of shear-compression failure which is regarded as one of typical shear failure modes. The design methods of reinforcement ratios with respect to steel bars and FRP grids mentioned before are introduced by GB 50010 [58], and they are determined by the following equations.

$$\rho_{web} = \frac{A_{web}}{b_{web} \cdot s} \tag{1}$$

$$\rho_w = \frac{A_w}{b_{web} \cdot h_0} \tag{2}$$

where, ρ_{web} , ρ_w are defined as the shear and tensile reinforcement ratio (i.e., the corresponding steel bars and FRP grids in this paper), respectively; s is defined as the spacing of the shear reinforcement; b_{web} and h_0 are defined as the cross-sectional width and effective depth of the specimens, respectively; and A_w and A_{web} are defined as the total cross-sectional area of the tensile reinforcement and shear reinforcement at a spacing of s , respectively.

A ready-mix normal concrete for casting and a kind of cementitious inorganic material called PCM for shotcrete were provided by local companies. For concrete, Ordinary Portland Cement (OPC, density: 3.14 g/cm³), sea sand (density: 2.59 g/cm³), crushed stone (density: 2.76 g/cm³) with maximum size of 20 mm, and water were used in the concrete mixture. The water-to-cement ratio and sand ratio of this concrete were 0.63 and 45.8%, respectively. PCM is a cementitious structural repairing mortar with higher tensile and compressive strength than other kinds of normal mortar, which consists of cement, styrene-butadiene rubber (SBR) polymer, and acrylic fiber, and the detailed mixture proportions of PCM are listed in Table 2. During the process of casting concrete and jetting PCM as continuous casting, three cubic samples (spaces between 150 mm) for concrete and three cubic samples (spaces between 70.7 mm) for PCM were reserved and then cured 28 days. The main mechanical properties (i.e., strength and elastic modulus) of concrete, PCM, steel bars, and CFRP grids follow their own standards of test methods [38,59–61], and then the average measured values of all material are summarized in Tables 3 and 4.

Table 2. PCM mixture proportion (kg/m³).

Water	Cement	Fly Ash	Sand	Acrylic Fiber	SBR Polymer
234	483		966	1.45	70

Table 3. Material properties of concrete and PCM.

Materials		f_c , MPa	f_t , MPa	E_c , GPa
Concrete	N0	22.4	2.04	24.4
	RWC5, RHWC5	22.2	2.38	24.5
PCM	RWC5, RHWC5	72.7	3.16	27.0

Note: f_c, f_t and E_c are the average compressive strength, tensile strength, and elastic modulus of the corresponding inorganic materials (i.e., concrete and PCM in this study), respectively.

Table 4. Material properties of steel bars and CFRP grids.

Types	Materials	A_{w1} , mm ²	f_{t0} , MPa	f_{y0} , MPa	E_0 , Gpa
HRB335	D32 Tensile steel bars	804.2	593	407	200
HRB335	D10 Stirrups	78.5	573	363	
CR5	CFRP grids	13.2	1400	-	100

Note: A_{w1} is the cross-sectional areas of a single steel bar or FRP grid; f_{t0}, f_{y0} are the mean values of the ultimate and yielding strengths, respectively.

2.2. Test Method

The beam specimens were subjected to two-point loading through the load spreader combining load plates and a load-spreader beam [62], which was placed between the specimen and the hydraulic actuator, as illustrated in Figure 4. The applied load, operated by a closed-loop servo-controlled hydraulic actuator of 2000 kN, was applied monotonically under a displacement control at a rate of 0.01 mm/s [63]. In addition, Figure 5 shows the geometrical dimensions of the specimens and the installation placement of the strain gauges. Strain gauges with base length of 3 mm were installed at several locations of the existing stirrups throughout the shear span. Meanwhile, some strain gauges were also installed on the vertical grids, which were near the measuring points of the existing stirrups, in order to reveal the shear strengthening effect of the CFRP grid. Moreover, a total of five linear variable differential transformers (LVDTs), with maximum range of 50 mm, were used to measure the vertical deflections of the beam specimens.

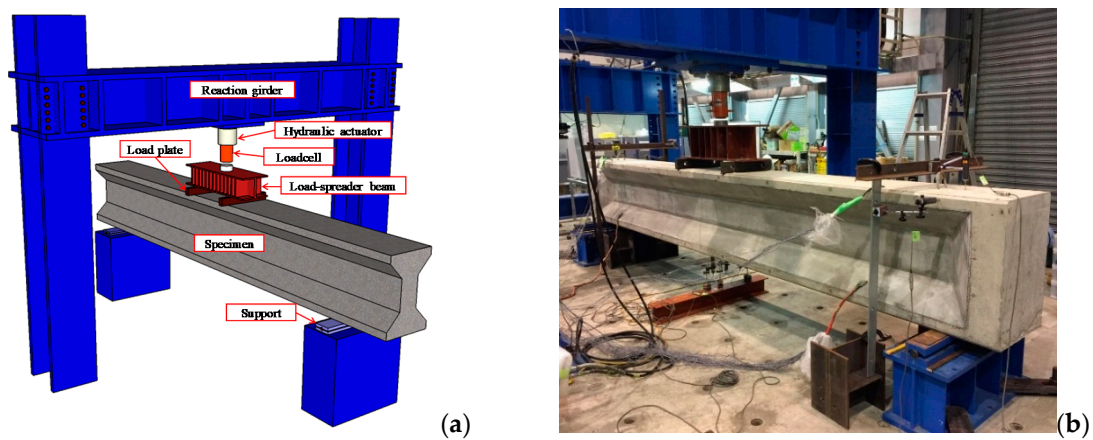


Figure 4. Test setup: (a) Schematic diagram; (b) Photo.

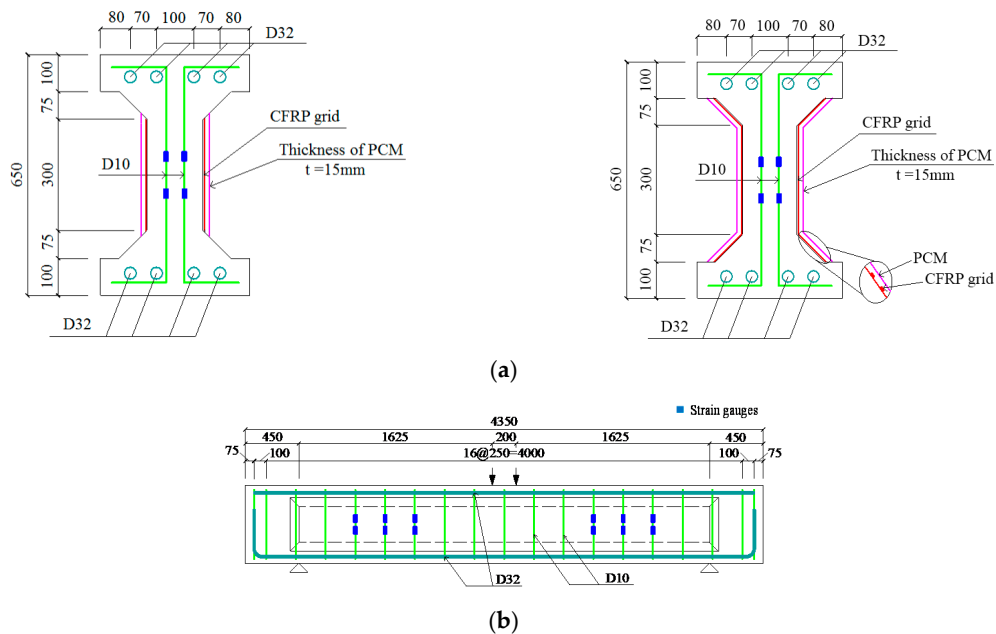


Figure 5. Cont.

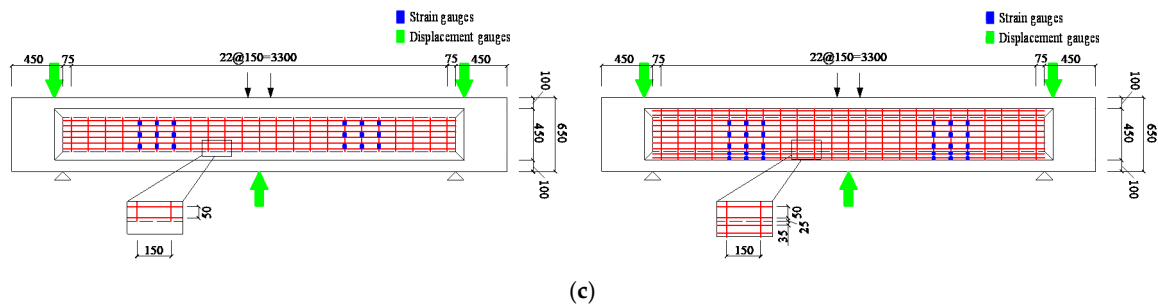


Figure 5. Schematic of specimens in Series A (Unit: mm): (a) Side view for strengthened beams (left side for RWC5, right side for RHWC5); (b) Front view for the reinforcement cage and the longitudinal section of the beam; (c) Front view for FRP grid area (left side for RWC5, right side for RHWC5).

2.3. Test Results and Discussion

The crack patterns of beam specimens on ultimate states and the load–deflection ($P-\delta$) responses are indicated in Figures 6 and 7, respectively. Moreover, the PCM material was stripped off as completely as possible after the specimens were damaged to observe the failure modes of the CFRP grid. In Figure 6, the pictures on the right correspond to the marked areas on the specimens, showing the grid. The typical shear-compression failure, regarded as the main failure mode, appeared in strengthened beams.

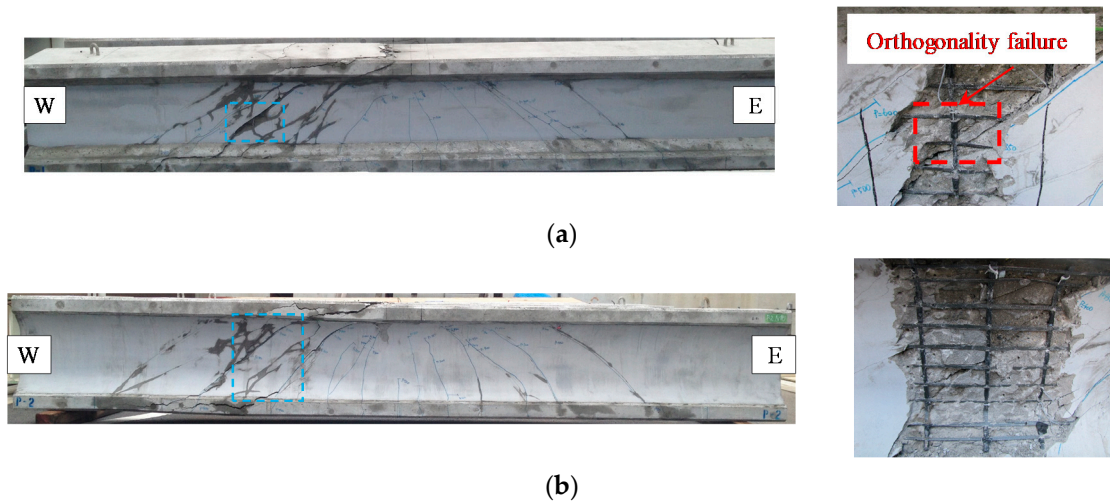


Figure 6. Crack patterns of strengthened beams: (a) RWC5; (b) RHWC5. The pictures on the right correspond to the marked areas (blue dashed rectangle) on the specimens, showing the grid.

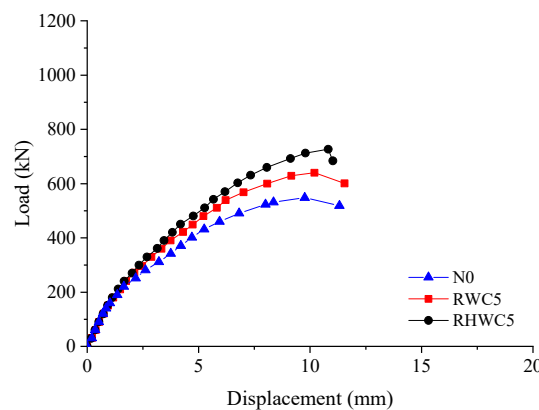


Figure 7. Load–deflection ($P-\delta$) responses.

According to Figure 7, specimen RHWC5 is obviously better than the others in this series tests, no matter in ultimate capacity, second stiffness, or even displacement of peak load level. In detail, when compared to the specimen without reinforcement (i.e., N0), the ultimate load of specimens with reinforcement, i.e., the specimen RWC5 and RHWC5, are improved by approximately 17% and 33%, respectively. It can be concluded that the CFRP grid-PCM reinforcement layer proposed for the strengthening of concave concrete is effective. Moreover, for specimen RHWC5, the slope of the P - δ relationship increases slightly and the ultimate load is increased by approximately 14% when the loading force is beyond 500 kN, in comparison with specimen RWC5. Therefore, better performance in both the second stiffness occurred and the ultimate load if an RC beam with an I-shaped profile is strengthened by CFRP grid-PCM layer along the web and haunch. On the other hand, the orthogonality failure of partial grids (red dashed rectangular pointed by an arrow) close to the critical shear cracks and the corresponding local debonding failure of PCM are shown in specimen RWC5, reconfirming that the strengthening approach for RC beam, which is externally bonded by the CFRP grid-PCM reinforcement layer along the web only, is not sufficient, in comparison with the web and haunch strengthening layer. It should be noted that the casting number of each type of beam was only one in this series; as a result, the disadvantages (e.g., the influence of a scatter range, the determination of the failure modes) caused by testing each configuration once are inevitable to some extent, but they are unlikely to deny the effectiveness of the results obtained with these beam specimens.

3. Experimental Study on Reinforcement Amount

3.1. Test Programme

According to the test results from the last section, better performance was obtained on concrete beams with I-shaped profile, especially in the ultimate state, when using reinforcement of CFRP grid-PCM layer along both the web and the haunch regions. Other bonding tests of FRP grid-PCM and concrete blocks have been previously conducted by authors, and these research results suggested that the bonding behavior between the existing concrete and the CFRP grid with PCM shotcrete was sufficient, while the essential number of grid points in one plane was at least three [44,64]. Thus, seven types of beam specimens with larger dimensions and full range reinforcement (i.e., both web and haunch), Series B, were prepared and then tested.

In this series, the reinforcement amount of the CFRP grids is considered as the main test variable to investigate their influence on RC beams strengthened by CFRP grid-PCM layer in shear, as indicated in Table 5. In terms of the existing portion, the stirrups spaced intervals of 250 mm were Grade HRB 300 steel bars with diameter of 10 mm, while the compressive and tensile steel bars were Grade HRB 335 with diameter of 35 mm. The shear span ratio is 2.93 in all beam specimens. For strengthened beams, in addition to control beam N0' with no reinforcement, all of strengthened beams are reinforced along the web and the haunch: the RHWP specimen reinforced by PCM only, specimens RHWC4, RHWC6, and RHWC8 reinforced with PCM and CFRP grids of different types (named as CR4, CR6 and CR8). The RHWC4' specimen includes a grid type CR4, but with vertical spacing of 50 mm, which is 1/3 of the others (150 mm). The remaining specimen, RHWC64, is special because it is reinforced by a combination of CR4 and CR6 types, layered in horizontal and vertical directions, respectively.

Some design principles and construction methods are almost the same as the previous Series A tests, including design concepts, manufacture process, standards for test methods, instrumentation, and testing procedure. Hence, these are not introduced again, and all related measured results are summarized in Tables 6 and 7, while the geometrical dimensions of specimens and the installation placement of the strain gauges are shown in Figure 8.

Table 5. Details of the beam specimens of Series B.

Type	Type of CFRP	Grid Interval (Vertical × Horizontal, mm)	Reinforcement Range	Thickness of PCM, mm
N0'	-	-	-	-
RHWP	-	-	Haunch + Web	20
RHWC4	CR4	150 × 50	Haunch + Web	20
RHWC6	CR6	150 × 50	Haunch + Web	20
RHWC8	CR8	150 × 50	Haunch + Web	20
RHWC4'	CR4	50 × 50	Haunch + Web	20
RHWC64	CR6&CR4	150 × 50	Haunch + Web	20

Table 6. Material properties of concrete and PCM.

	Materials	f_c , MPa	f_t , MPa	E_c , GPa
Concrete	N0', RHWP	23.9	2.07	23.5
	RHWC4, RHWC6, RHWC8, RHWC4', RHWC64	26.8	2.09	24.5
PCM	RHWP	50.9	3.16	24.5
	RHWC4, RHWC6, RHWC8, RHWC4', RHWC64	54.3	3.16	24.5

Note: f_c , f_t , and E_c are the average compressive strength, tensile strength, and elastic modulus of the corresponding inorganic materials (i.e., concrete and PCM in this study), respectively.

Table 7. Material properties of steel bars and CFRP grids.

Types	Materials	A_{w1} , mm ²	f_{t0} , MPa	f_{y0} , MPa	E_0 , Gpa
D35	tensile steel bars	956.6	578	386	200
D10	Stirrups	71.33	573	363	
CR4	CFRP grids	6.6	1400	-	100
CR6		17.5	1400	-	100
CR8		26.4	1400	-	100

Note: A_{w1} is the cross-sectional areas of single steel bar or FRP grid; f_{t0} , f_{y0} are the mean values of the ultimate and yielding strengths, respectively.

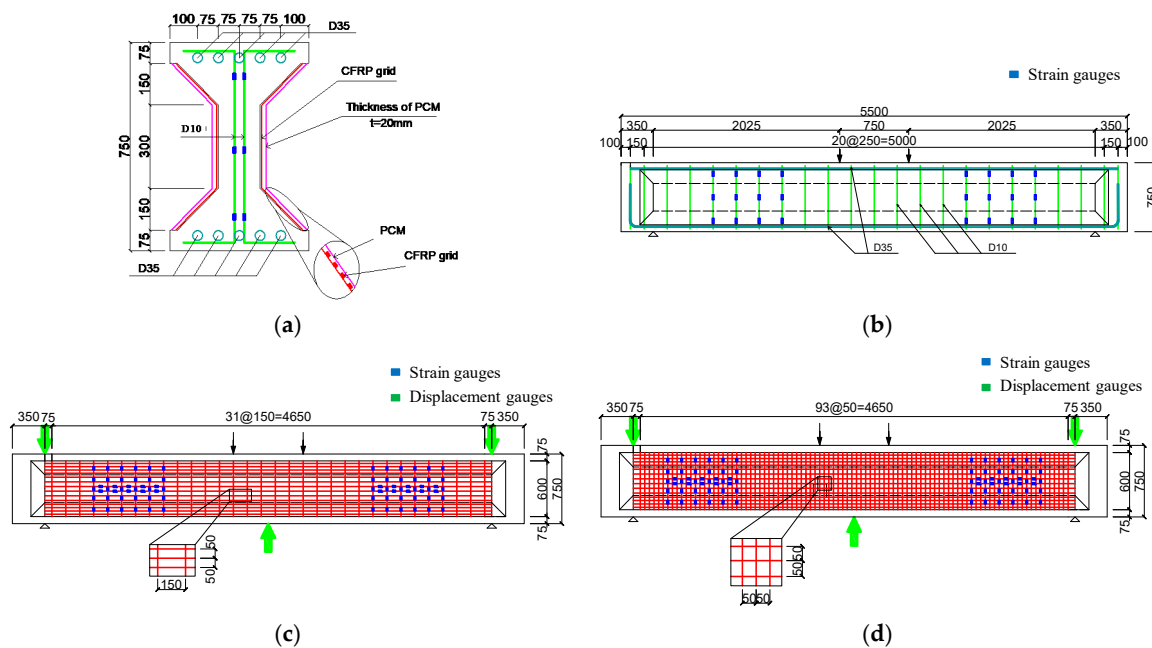


Figure 8. Schematic of specimens in Series B (Unit: mm): (a) Side view for strengthened beams with FRP grid; (b) Front view for reinforcement cage and the longitudinal section of the beam; (c) Front view for FRP grid area (150 mm × 50 mm, i.e., RHWC4, RHWC6, RHWC8, RHWC64); (d) Front view for FRP grid area (50 mm × 50 mm, i.e., RHWC4').

3.2. Results and Discussion

3.2.1. Failure Modes

The summary of the experimental results and the crack patterns of beam specimens regarding the ultimate load are presented in Table 8 and Figure 9, respectively. Similar to the analysis of Series A (Figure 6), the PCM material was stripped off from strengthened beam specimens as completely as possible after loading tests were finished. All beams failed in a typical shear-compression failure, which is concrete crushing after the main shear cracks developed completely, as shown in Figure 9. During the whole loading process, although fine flexural cracks were observed on the lateral surface at a load level of approximately 240 kN, the critical shear crack along the diagonal direction connecting the support and loading point appeared at various loads with the changes in the reinforcement amount of the CFRP grid. In addition, as load increased, the length and width of the flexural and shear cracks developed gradually for all beam specimens, but an increase in the number of cracks with smaller width were observed on the outside surface when RC beams were strengthened by PCM as a thin covering. As predicted, the local concrete crushing occurred on the upper edge of the RC beam.

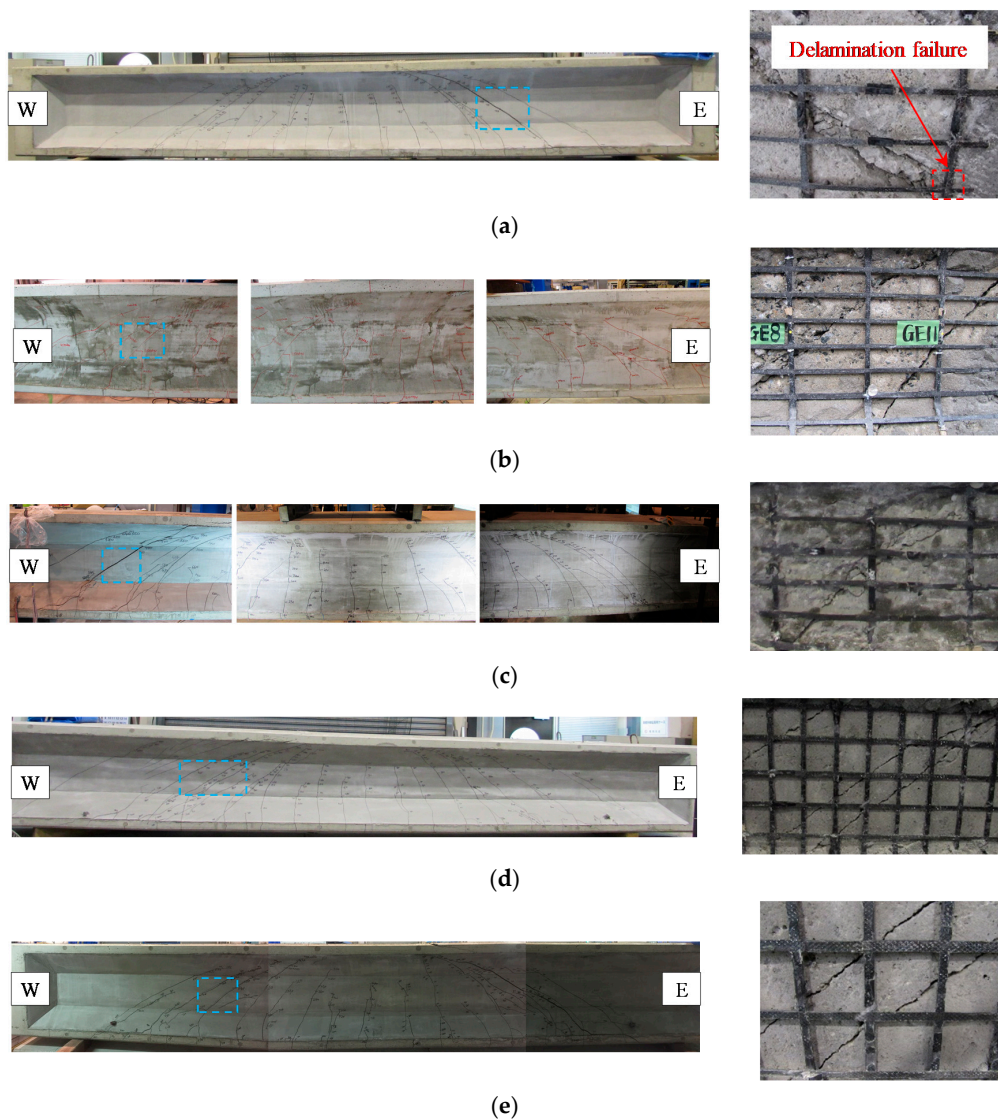


Figure 9. Crack patterns: (a) RHWC4; (b) RHWC6; (c) RHWC8; (d) RHWC4'; (e) RHWC64. The pictures on the right correspond to the marked areas (blue dashed rectangle) on the specimens, showing the grid.

Table 8. Summary of experimental results.

Types	P_{fc} , kN	P_{sc} , kN	P_u , kN	η_u , %	Failure Mode
N0'	240	332	665	-	SC
RHWP	242	392	677	1.8	SC
RHWC4	242	421	881	32.5	SC
RHWC6	240	450	949	42.7	SC
RHWC8	239	481	943	41.8	SC + PD
RHWC4'	242	462	950	42.9	SC
RHWC64	241	433	860	29.3	SC + PD

Note: P_{fc} —the first flexural cracking load, P_{sc} —the critical shear cracking load, P_u —the ultimate load, η_u —the increase ratio of ultimate load, SC—shear-compression failure, PD—partial debonding of CFRP grid.

As exhibited in Table 7, the load value at which the first flexural cracking happens (P_{fc}) stays similar for all specimens, as expected. For the specimen RHWP reinforced by PCM only, the ultimate load value (P_u) shows little increase in comparison with specimen N0', but the value at which the shear cracks appear (P_{sc}) is higher due to the existence of the PCM layer. The enlargement of the cross-sectional areas of CFRP grid (i.e., specimens RHWC4 and RHWC6) causes the magnitudes of both P_{sc} and P_u to increase gradually with the cross-sectional areas of CFRP. The same strengthening effect due to the reduction in grid spacing is observed comparing specimens RHWC4 and RHWC4' (with one-third the transverse grid spacing). The specimen RHWC8 shows, on the one side, an increase of the P_{sc} value in respect to specimen RHWC6, but almost the same ultimate load level P_u , caused by the debonding phenomenon, and despite the largest cross-sectional area involved. Specimen RHWC64 is similar to specimen RHWC8 in terms of CFRP cross-sectional area involved. However, the debonding failure occurs prior to the upper concrete crushing, leading to an ultimate load value lower than any other CFRP grid-PCM layer strengthened specimen. The delamination failure type and the rupture of the CFRP grid has not been observed in Series B, except for specimen RHWC4 (see Figure 9a), which shows the delamination failure of the partial CFRP grids (red dashed rectangular pointed by an arrow) that were near the critical shear crack.

3.2.2. Load–deflection (P – δ) Responses

The load–deflection (P – δ) values for the experimental specimens are plotted in Figure 10. Overall, the trend of the load–deflection responses contains one clearly visible inflection point changing the curve stiffness at load values of about 200 kN, corresponding to the first flexural cracking loads. A less clear inflection, but analyzed in data, occurs at about 500 kN, corresponding to the critical shear cracking. In addition, the initial fine flexural and shear cracks were observed during the test and then developed gradually on the surface of specimens as the loading value increased.

When compared to the control beam (i.e., N0'), the ultimate load capacity and the curve stiffness are almost same to the specimen only reinforced by PCM (i.e., RHWP), indicating that little shear resistance contribution for load-carrying capacity is provided by PCM. The load capacity of specimens reinforced by the CFRP grid-PCM (i.e., RHWC4, RHWC6, RHWC8, RHWC4', RHWC64) layer are improved in a range from 29.3 to 42.9% in comparison with the control beam (i.e., N0'), thus it can be noted that the strengthening effect of the CFRP grid is adequate. Furthermore, compared to specimen RHWC4, the ultimate load capacity of specimen RHWC8 and RHWC4' increase by approximately 7% and 8%, respectively, demonstrating that the ultimate load capacity increases with the cross-sectional area's increase and the spacing decrease of the vertical grids. However, once debonding failure occurs at the interface between the CFRP grid and concrete substrate during the whole loading process, as observed for specimen RHWC64, there is a decline in the ultimate load.

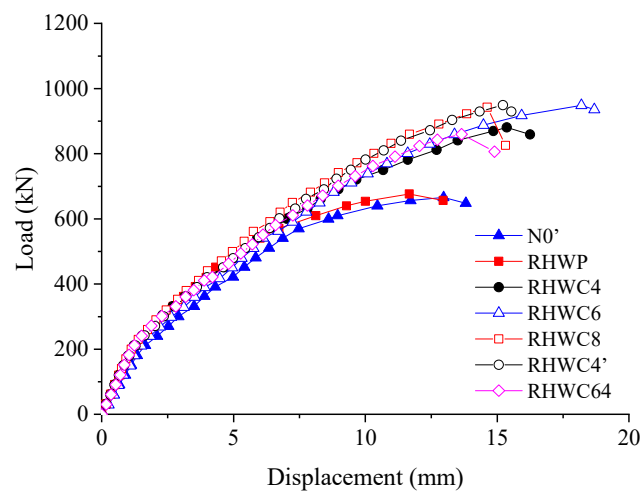


Figure 10. Load–deflection (P – δ) responses of Series B.

3.2.3. Load–strain (P – ϵ) Responses

The load–strain (P – ϵ) responses for each specimen are presented in Figure 11. The values plotted in each case correspond to the strain measured with strain gauges located at the positions indicated in the inserts of each panel, labelled as S for the cases with no CFRP reinforcement and G for the CFRP reinforced specimens. The S and G positions are given in respect to the bearing and the load application points. In panel (a), the results show that the ultimate stirrup strains of the control beam (i.e., N0') greatly exceed their yielding strain. For specimen RHWP, which is reinforced by PCM only, the stirrup strains increase gradually with the increase of the loading values but are not greater than the yielding strain at the end of the test. In addition, the P – δ responses of the CFRP grids present similar behavior to those of stirrups; meanwhile, the stiffness curves are larger than those of the control beams before the stirrups reach their yielding strain, so it can be concluded that the synergistic effect between the grids and concrete is obvious. Therefore, the shear force is primarily resisted by the stirrups in combination with the CFRP grids. In terms of specimens RHC4, RHC6, and RHC8 (panels a, b, and c, respectively), the corresponding ultimate strain of the CFRP grid increases with the reduction of the cross-sectional area. On the other hand, the ultimate strain climbs as the spacing of the vertical grids increases, which can be found through comparing specimens RHC4 and RHC4' (panels b and e, respectively), demonstrating that better deformation performance and CFRP grid efficiency are obtained when the reinforcement ratio of the CFRP grid is reduced. From this perspective, the conclusion can be drawn that delamination or debonding of the CFRP from the surrounding PCM (a second possible phenomenon) can be excluded, implying that local debonding occurred at the interface between FRP grids and the concrete substrate, rather than between the FRP grids and PCM. Similar results were also obtained by other studies [65,66]. Overall, none of the FRP grids' strain reached rupture strain, as measured by uniaxial tensile tests when various load levels of strengthened beams arrived at ultimate states. In addition, the greatest number of cracks appear in RHC4' due to the minimum spacing of the CFRP grid in comparison with the others. Furthermore, the partial grid strains abruptly and dramatically become small (the ultimate strain is equal to the debonding strain at this time), and it can be concluded that the debonding failure occurs at the interface between the CFRP grid and the concrete substrate prior to the rupture of the CFRP grid.

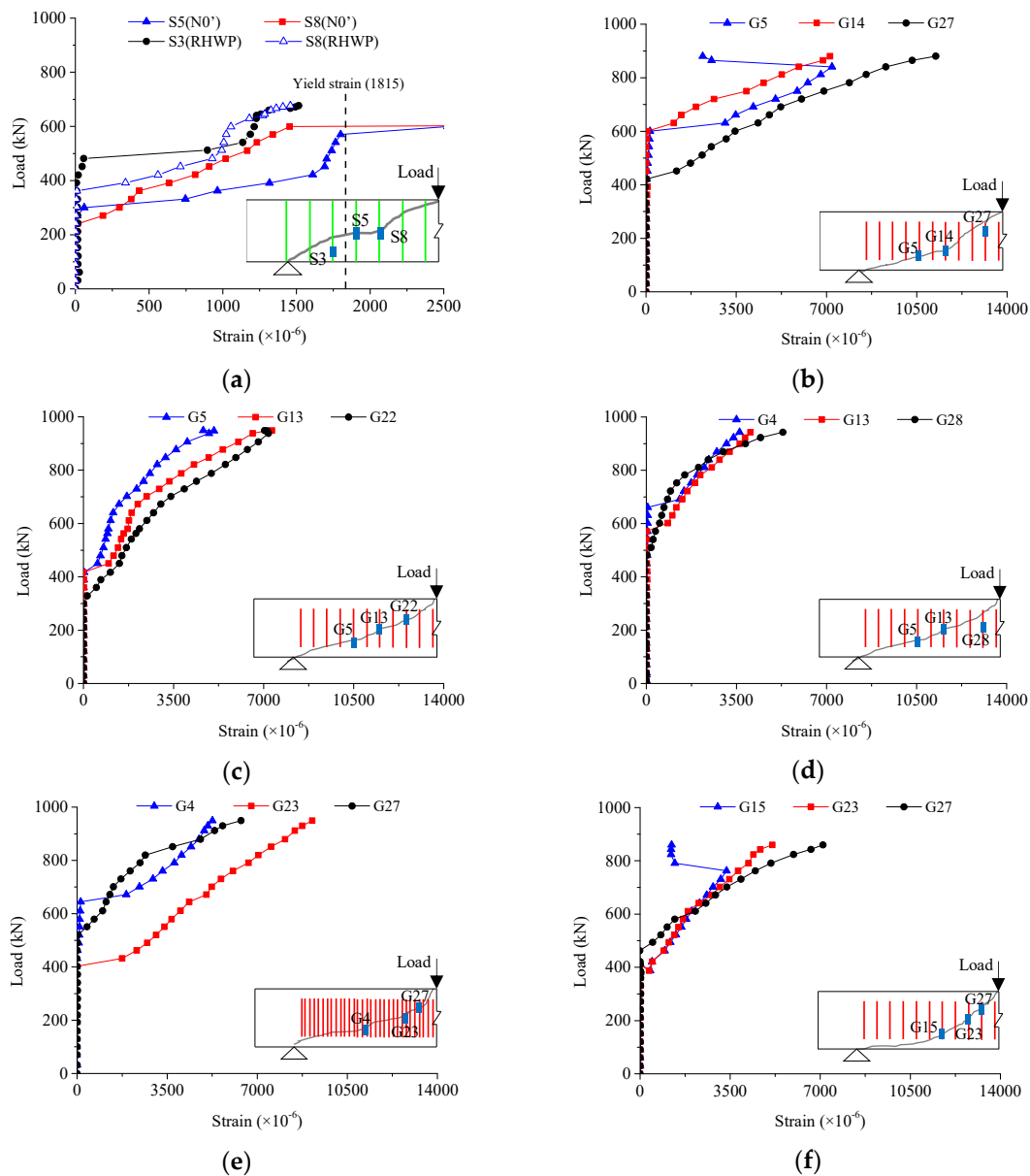


Figure 11. Load–strain ($P-\epsilon$) responses: (a) $N0'$ and RHWP; (b) RHWC4; (c) RHWC6; (d) RHWC8; (e) RHWC4'; (f) RHWC64. The insert at each panel indicates the location of the strain gauges measured and shown in each plot.

4. Analytical Model of Shear Capacity

To predict the shear capacity of RC beams with a CFRP-PCM reinforcement layer, the following Equation (3) is usually used as the analytical system to obtain the shear capacity of strengthened beams (V), which is introduced by the Japan Road Association [67], given as follows:

$$V = V_{con} + V_{pcm} + V_{st} + V_g \tag{3}$$

where V_{con} , V_{pcm} , V_{st} , and V_g are defined as the shear resistance contribution of the concrete, PCM, stirrups, and CFRP grid, respectively. It should be pointed out that the design method of PCM on shear contribution is very similar to concrete, according to previous experiments together with standards suggested [66,67], and this corresponding equation for PCM hence would not appear over and over;

rather, a small amount of difference would still be noted. All the mentioned parameters can be expressed as:

$$V_{con}(V_{PCM}) = \frac{\beta_d \cdot \beta_p \cdot \beta_n \cdot f_{vcd} \cdot b_{web} \cdot h_0}{\gamma_b} \tag{4}$$

where γ_b is defined as the reduction factor of member coefficient and the recommended value is equal to 1.00; while the calculation methods for f_{vcd} and for coefficients β_d and β_p are:

$$\beta_d = \sqrt[4]{\frac{1000}{h_0}} \tag{5}$$

$$\beta_p = \sqrt[3]{100\rho_w} \tag{6}$$

$$f_{vcd} = 0.20 \sqrt[3]{f'_c} \tag{7}$$

where f'_c is defined as the design compressive strength of concrete or PCM; ρ_w is calculated by the Equation (2), as well as h_0 , both mentioned in Section 2.1. The parameter β_n , depending on the bending moment and the stress produced by axial forces, has value $\beta_n = 1$, since in this study no prestress is introduced.

The stirrup contribution is given by:

$$V_{st} = \frac{A_{web} \cdot f_{y0} \cdot (\sin \alpha + \cos \alpha) \cdot z}{s \cdot \gamma_b} \tag{8}$$

where, α is defined as the angle between the stirrups and the longitudinal direction of the member; f_{y0} and A_{web} are defined as the yielding strength and cross-sectional areas in terms of internal stirrups here; z is defined as the ratio of the effective depth to the constant value 1.15; and coefficient value γ_b is equal to 1.15.

The CFRP grid contribution is given by:

$$V_g = \frac{A'_{web} \cdot E_0 \cdot \varepsilon_u \cdot (\sin \alpha_s + \cos \alpha_s) \cdot z}{s_g \cdot \gamma_b} \tag{9}$$

where A'_{web} and E_0 are defined as the cross-sectional areas and elastic modulus with respect to vertical FRP grids regarded as the shear reinforcement here; α_s is defined as the angle between the CFRP grid and transverse direction of the member; ε_u is defined as the rupture strain of the CFRP grid; s_g is defined as the spacing of the vertical grids, which are generally considered as external stirrups for better understanding; and the coefficient value γ_b is equal to 1.15.

The strengthened beam specimens are subjected to shear force during the whole loading process, and it is worth noting that some scholars have proposed that the debonding failure of FRP composites generally occurred at the interface prior to concrete crushing [49,68,69]. It can be observed from the experimental results that the local debonding failure occurred at the interface between the CFRP grid and the concrete in advance of the rupture of the CFRP grid. Therefore, the shear capacity evaluation method for concrete beams reinforced by a CFRP grid-PCM reinforcement layer, which is based on the effective strain of FRP rod introduced by JSCE's Concrete Library [70], needs to be utilized, and the expression of corresponding effective strain is represented as follows:

$$\varepsilon_{u,rod} = \sqrt{f'_{mcd} \frac{\rho_w E_s}{\rho_{web} E_g}} \cdot \left[1 + 2 \left(\frac{\sigma'_N}{f'_{mcd}} \right) \right] \times 10^{-4} \tag{10}$$

where ρ_{web} , ρ_w are defined in Equations (1) and (2), respectively, E_s is defined as the elastic modulus of the tensile steel bars; E_g is defined as the elastic modulus of FRP rods and thus vertical FRP grids are used instead; f'_{mcd} and σ'_N are defined as the design compressive strength of concrete considering the

size effect from the specimens and the average value of the axial compressive strength, respectively. The values of f'_{mcd} and σ'_N are determined as:

$$f'_{mcd} = \left(\frac{h}{0.3}\right)^{-\frac{1}{10}} \cdot f'_c \tag{11}$$

$$\sigma'_N = \frac{N'_d + P_{ed}}{A} \tag{12}$$

where P_{ed} is defined as the effective tensile force of reinforcement in the axial direction; N'_d is defined as the design bending moment and axis compressive force; A and h are defined as the total cross-sectional area and the height of the specimen, respectively.

Using the effective strain defined in Equation (10), it is possible to evaluate the shear value V according to Equation (3). Comparing the calculated shear ($V_{cal,rod}$) with the experimental ultimate shear capacity (P_{exp}), a safety ratio is defined. In Table 9, the values of $V_{cal,rod}$, P_{exp} and safety ratios are listed, corresponding to the experimental values of this study and some collected data from other results [37,51,71]. The safety ratio values are in the range of 1.16 to 1.61 considering all strengthened beams. These values are much higher than 1.0, indicating that the method based on the effective strain of the FRP rod can be used to evaluate the shear capacity of RC beams using a CFRP grid and PCM layer. Similarly, the values of the effective strain can be evaluated from the experimental values of maximum strain of the CFRP grid ($\epsilon_{p,max}$) listed in Table 9. The values increase with the reduction of the cross-sectional area of the CFRP grid. It can be seen that the smaller cross-sectional areas are, the better the deformation performance of the CFRP grid. If these strains are compared with the strains obtained by Equation (10) for the FRP rod (listed in Table 9), the values are much higher. This is because the FRP grid can resist higher shear force by vertical grids, horizontal grids, and grid points (as the intersections of vertical and horizontal grids), meaning that both vertical and horizontal grids have an inherent relation rather than only a single vertical direction of FRP grids working like an FRP rod. For this reason, there is a great difference between their load-transferring mechanisms; this can explain why the previous calculation system can be used to predict the shear capacity, but always being over-predictive.

Table 9. Comparison between calculated value $V_{cal,rod}$ results and the corresponding experimental values.

Series	Type	Experimental Value P_{exp}		Calculated Value $V_{cal,rod}$		$P_{exp}/V_{cal,rod}$
		P_{exp} (kN)	$\epsilon_{p,max}$ ($\times 10^{-6}$)	$V_{cal,rod}$ (kN)	$\epsilon_{u,rod}$ ($\times 10^{-6}$)	
Series A	RWC5	640	10,533	552	3449	1.16
	RHWC5	727	7853	559	3449	1.30
Series B	RHWC4	881	10,757	636	5494	1.39
	RHWC6	949	7188	684	3374	1.39
	RHWC8	943	5467	712	2747	1.33
	RHWC4'	950	7412	674	3172	1.41
	RHWC64	860	6981	684	3374	1.26
Literature [50]	SB1	376	2100 *	234	2428	1.61
Literature [36]	L3	373	4004	237	1833	1.57
Literature [71]	SB2-3	409	2500 *	246	1684	1.66
	SB3-5	351	3400 *	254	1218	1.38

Note: symbol * means the actual value beyond the value shown in this table.

Therefore, a better evaluation method of shear capacity for concrete beams with CFRP grids should be developed to calculate or predict shear capacity more accurately than by using the previous method. To replace the effective strain corresponding to the FRP rod, the ultimate strain value of the FRP grid ($\epsilon_{u,grid}$) has been defined as the measured ultimate or debonding strain of the CFRP grid

(also called effective strain of CFRP grid [38,40]) and has been explored through regression analysis, in two series of tests. The analysis is shown in Figure 12 and the result is given as:

$$\epsilon_{u,grid} = \left(\frac{1}{0.0352\rho_g + 0.0079} \right)^2 \times 10^{-6} \tag{13}$$

where ρ_g is defined as the cross-sectional area of the CFRP grid per unit length in the horizontal direction.

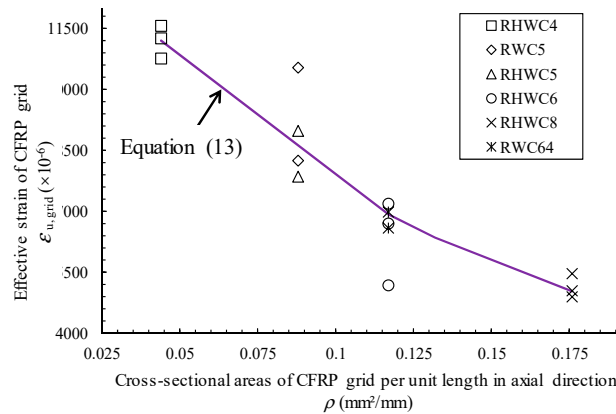


Figure 12. Effective strain of vertical CFRP grid.

Considering the new definition for the strain, the values for shear can be re-evaluated (labelled as $V_{cal,grid}$ and shown in Appendix A) and compared with those obtained previously ($V_{cal,rod}$) in Table 9. The comparison is plot as the chart of Figure 13a. Again, the safety ratios of P_{exp} to $V_{cal,grid}$ are beyond 1.00 so they satisfy the safety requirement. Similarly, the strain value ($\epsilon_{u,grid}$) can be re-evaluated, and the values result much closer to the measured ones, as shown in Figure 13b. It can be deduced that the latter calculated system, which is proposed to evaluate the shear capacity for concrete beams externally bonded with a CFRP grid-PCM reinforcement layer, is demonstrated to be a more reasonable approach than the previous method.

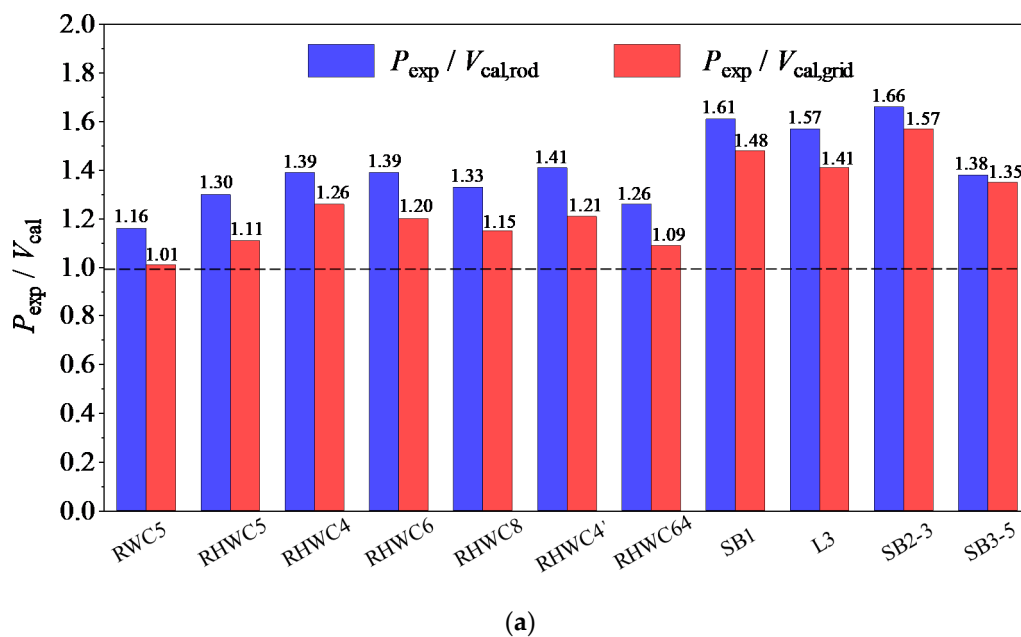


Figure 13. Cont.

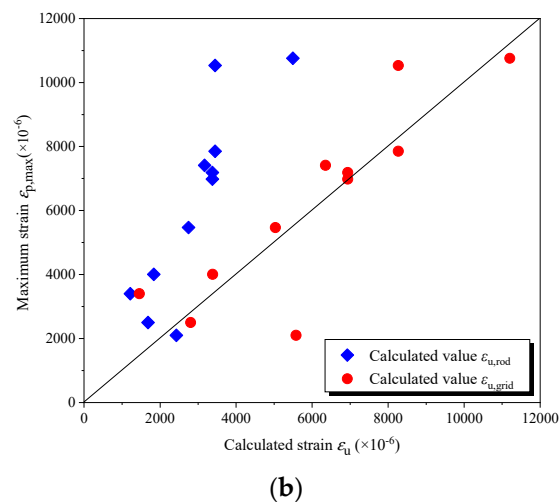


Figure 13. Comparison between the calculated and corresponding experimental values: (a) Comparison of shear capacity; (b) Comparison of CFRP grid strain.

5. Conclusions

- (1) CFRP grids close to the shear cracks show orthogonal failure and the corresponding PCM experiences debonding failure when the specimen is strengthened on the web to resist shear force. It can be deduced that the shear strengthening effect of the CFRP grid-PCM reinforcement layer is insufficient if the RC beam is only reinforced by a strengthening layer on the web.
- (2) Compared to the specimen with a reinforcement layer only in the web, better performances of specimens reinforced in both the web and haunch regions are obtained in terms of the second stiffness and the ultimate shear capacity, reconfirming that the CFRP grid-PCM layer used for the full sectional reinforcement of RC beams with an I-shaped profile is indispensable.
- (3) The shear capacity is improved by 30–40% in specimens strengthened by a CFRP grid-PCM reinforcement layer. Considering the limited contribution of the PCM layer alone, the conclusion is that the shear strengthening of RC beams with CFRP grid-PCM layer is obvious and is primarily provided by the FRP grid.
- (4) Better synergistic deformation of the CFRP grid is obtained when the corresponding reinforcement amount is reduced. On the other hand, delamination or debonding of the CFRP from the surrounding PCM can be excluded.
- (5) Local debonding failure usually occurs at the FRP grid–concrete interface prior to the rupture of the CFRP grid. In addition, using the effective strain of the FRP rod to predict the effective/actual strain for the CFRP grid can be considered to be secure, but is somewhat over-predictive.
- (6) A new evaluation method based on the CFRP grid's effective strain has been developed in this paper. According to a series of experimental results and collected data from other results, this novel evaluation method is validated and a more effective and reasonable approach for predicting the shear capacity of RC beams using a CFRP grid-PCM layer is obtained.

Author Contributions: Data curation, R.G. and S.H.; software, L.C.; visualization, L.C.; writing—original draft preparation, L.C.; writing—review and editing, R.G. and B.W.; supervision, R.G.; funding acquisition, R.G.

Funding: This research was supported by the Fundamental Research Funds for the Central Universities (grant number: 2682018CX06) and the Key Laboratory Opening Project of Southwest Jiaotong University (grant number: ZD201918018).

Acknowledgments: The authors are grateful for the technical support from FRP Grid Method Association at Japan. They would also like to acknowledge the relevant staff of Kyushu University that make a huge contribution to all experimental tests.

Conflicts of Interest: The authors declare no conflict of interest about the research and the publication of this paper.

Appendix A

The following table contains details and supplementary data to Figure 13 of the main text.

Table A1. Comparison between calculated value $V_{cal,grid}$ and the corresponding experimental values.

Series	Type	Experimental Value P_{exp}		Calculated Value $V_{cal,grid}$		$P_{exp}/V_{cal,grid}$
		P_{exp} (kN)	$\epsilon_{p,max}$ ($\times 10^{-6}$)	$V_{cal,grid}$ (kN)	$\epsilon_{u,grid}$ ($\times 10^{-6}$)	
Series A	RWC5	640	10,533	634	8268	1.01
	RHWC5	727	7853	655	8268	1.11
Series B	RHWC4	881	10,757	701	11,200	1.26
	RHWC6	949	7188	792	6937	1.20
	RHWC8	943	5467	819	5033	1.15
	RHWC4'	950	7412	784	6352	1.21
	RHWC64	860	6981	792	6937	1.09
Literature [50]	SB1	376	2100 *	254	5576	1.48
Literature [36]	L3	373	4004	265	3383	1.41
Literature [71]	SB2-3	409	2500 *	261	2805	1.57
	SB3-5	351	3400 *	260	1456	1.35

Note: symbol * means actual value beyond the value shown in this table.

References

- Bournas, D.A.; Pavese, A.; Tizani, W. Tensile capacity of FRP anchors in connecting FRP and TRM sheets to concrete. *Eng. Struct.* **2015**, *82*, 72–81. [[CrossRef](#)]
- Tetta, Z.C.; Bournas, D.A. TRM vs. FRP jacketing in shear strengthening of concrete members subjected to high temperatures. *Compos. Part B Eng.* **2016**, *106*, 190–205. [[CrossRef](#)]
- Akhoundi, F.; Vasconcelos, G.; Lourenço, P. In-plane behavior of cavity masonry infills and strengthening with textile reinforced mortar. *Eng. Struct.* **2018**, *156*, 145–160. [[CrossRef](#)]
- Wang, X.; Ghiassi, B.; Oliveira, D.V. Modelling the nonlinear behaviour of masonry walls strengthened with textile reinforced mortars. *Eng. Struct.* **2017**, *134*, 11–24. [[CrossRef](#)]
- Tetta, Z.C.; Koutas, L.N.; Bournas, D.A. Shear strengthening of full-scale RC T-beams using textile-reinforced mortar and textile-based anchors. *Compos. Part B Eng.* **2016**, *95*, 225–239. [[CrossRef](#)]
- Koutas, L.N.; Tetta, Z.; Bournas, D.A.; Triantafyllou, T.C. Strengthening of Concrete Structures with Textile Reinforced Mortars: State-of-the-Art Review. *J. Compos. Constr.* **2019**, *23*. [[CrossRef](#)]
- Alabdulhady, M.Y.; Sneed, L.H.; Carloni, C. Torsional behavior of RC beams strengthened with PBO-FRCM composite—An experimental study. *Eng. Struct.* **2017**, *136*, 393–405. [[CrossRef](#)]
- Gonzalez-Libreros, J.H.; Sneed, L.H.; D'Antino, T.; Pellegrino, C. Behavior of RC beams strengthened in shear with FRP and FRCM composites. *Eng. Struct.* **2017**, *150*, 830–842. [[CrossRef](#)]
- Gonzalez-Libreros, J.H.; Sabau, C.; Sneed, L.H.; Pellegrino, C.; Sas, G. State of research on shear strengthening of RC beams with FRCM composites. *Constr. Build. Mater.* **2017**, *149*, 444–458. [[CrossRef](#)]
- Wakjira, T.G.; Ebead, U. FRCM/internal transverse shear reinforcement interaction in shear strengthened RC beams. *Compos. Struct.* **2018**, *201*, 326–339. [[CrossRef](#)]
- Dorota, M.; Tomasz, T.; Michał, M. Shear strengthening of reinforced concrete beams with PBO-FRCM composites with anchorage. *Compos. Part B Eng.* **2019**, *158*, 149–161.
- Younis, A.; Ebead, U.; Shrestha, K.C. Different FRCM systems for shear-strengthening of reinforced concrete beams. *Constr. Build. Mater.* **2017**, *153*, 514–526. [[CrossRef](#)]
- Truong, B.T.; Bui, T.T.; Limam, A. Experimental investigations of reinforced concrete beams repaired/reinforced by TRC composites. *Compos. Struct.* **2017**, *168*, 826–839. [[CrossRef](#)]

14. Scheerer, S.; Zobel, R.; Müller, E.; Senckpiel-Peters, T.; Schmidt, A.; Curbach, M. Special Issue “Textile Reinforced Cement Composites: New Insights in Structural and Material Engineering”. *Appl. Sci.* **2019**, *18*, 1322. [[CrossRef](#)]
15. Brückner, A.; Ortlepp, R.; Curbach, M. Textile reinforced concrete for strengthening in bending and shear. *Mater. Struct.* **2006**, *39*, 741–748. [[CrossRef](#)]
16. Yu, Y.L.; Yin, S.P.; Na, M.W. Bending performance of TRC-strengthened RC beams with secondary load under chloride erosion. *J. Cent. South Univ.* **2019**, *26*, 196–206. [[CrossRef](#)]
17. Thermou, G.E.; Papanikolaou, V.K.; Lioupis, C.; Hajirasouliha, I. Steel-Reinforced Grout (SRG) strengthening of shear-critical RC beams. *Constr. Build. Mater.* **2019**, *216*, 68–83. [[CrossRef](#)]
18. Thermou, G.E.; Hajirasouliha, I. Compressive behaviour of concrete columns confined with steel-reinforced grout jackets. *Compos. Part B Eng.* **2018**, *138*, 222–231. [[CrossRef](#)]
19. Lu, X.Z.; Ye, L.P.; Teng, J.G. Meso-scale finite element model for FRP sheets/plates bonded to concrete. *Eng. Struct.* **2005**, *27*, 564–575. [[CrossRef](#)]
20. Hawileh, R.A.; Rasheed, H.A.; Abdalla, J.A. Behavior of reinforced concrete beams strengthened with externally bonded hybrid fiber reinforced polymer systems. *Mater. Des.* **2014**, *53*, 972–982. [[CrossRef](#)]
21. Singh, S.B.; Vummadisetti, S.; Chawla, H. Influence of curing on the mechanical performance of FRP laminates. *J. Build. Eng.* **2018**, *16*, 1–19. [[CrossRef](#)]
22. Wei, Y.; Ji, J.; Zhang, M. Experimental investigation on tensile performance of FRP grids and its application as strengthening materials for underwater concrete. *Fiber Reinf. Plast. Compos.* **2014**, *47*, 10–15.
23. Osman, B.H.; Wu, E.; Ji, B.; Abdulhameed, S.S. Effect of reinforcement ratios on shear behavior of concrete beams strengthened with CFRP sheets. *HBRC J.* **2018**, *14*, 29–36. [[CrossRef](#)]
24. Vuggumudi, S.; Alagusundaramoorthy, P. FRP Strengthened RC rectangular Columns Under Combined Axial and Lateral Loading: Analytical Study. *Structures* **2018**, *14*, 88–94. [[CrossRef](#)]
25. Guo, R.; Pan, Y.; Cai, L.H.; Hino, S. Study on design formula of shear capacity of RC beams reinforced by CFRP grid with PCM shotcrete method. *Eng. Struct.* **2018**, *166*, 427–440. [[CrossRef](#)]
26. Ye, L.P.; Feng, P. Applications and development of fiber-reinforced polymer in engineering structures. *China Civ. Eng. J.* **2006**, *39*, 25–37.
27. Zhu, H.; Dong, Z.; Wu, G. Experimental study and theoretical calculation on the flexural stiffness of concrete beams reinforced with FRP bars. *China Civ. Eng. J.* **2015**, *48*, 44–53.
28. Colajanni, P.; Domenico, F.D.; Recupero, A.; Spinella, N. Concrete columns confined with fiber reinforced cementitious mortars: Experimentation and modelling. *Constr. Build. Mater.* **2014**, *52*, 375–384. [[CrossRef](#)]
29. Gao, W.Y.; Teng, J.G.; Dai, J.G. Effect of temperature variation on the full-range behavior of FRP-to-concrete bonded joints. *Compos. Struct.* **2012**, *16*, 671–683. [[CrossRef](#)]
30. Bernat, M.E.; Escrig, C.; Aranha, C.A.; Gil, L. Experimental assessment of textile reinforced sprayed mortar strengthening system for brickwork wallettes. *Constr. Build. Mater.* **2014**, *50*, 226–236. [[CrossRef](#)]
31. Azam, R.; Soudki, K.; West, J.S.; Noël, M. Shear strengthening of RC deep beams with cement-based composites. *Eng. Struct.* **2018**, *172*, 929–937. [[CrossRef](#)]
32. Zheng, W.Z.; Zhu, J. Progress of research on concrete structures strengthened with CFRP sheets bonded with inorganic cementitious materials. *J. Build. Struct.* **2013**, *34*, 1–12.
33. Yang, X.; Gao, W.Y.; Dai, J.G. Flexural strengthening of RC beams with CFRP grid-reinforced ECC matrix. *Compos. Struct.* **2018**, *189*, 9–26. [[CrossRef](#)]
34. Zheng, Y.Z.; Wang, W.W.; Brigham, J.C. Flexural behavior of reinforced concrete beams strengthened with a composite reinforcement layer: BFRP grid and ECC. *Constr. Build. Mater.* **2016**, *115*, 424–437. [[CrossRef](#)]
35. Wu, H.C.; Teng, J. Concrete confined with fiber reinforced cement based thin sheet composites. In *FRPRCS-6 Fiber Reinforced Polymer Reinforcement for Concrete Structures*; McGraw-Hill: Singapore, 2003; pp. 591–600.
36. Chen, W.Y.; Chen, X.B.; Ding, Y. The shear behavior of beams strengthened with FRP grid. In *Proceedings of the 5th International Conference on FRP Composites in Civil Engineering*, Beijing, China, 27–29 September 2010.
37. Yamaguchi, K.; Guo, R.; Hino, S.; Miyano, N. Shearing capacity and adhesive characteristic of reinforced interface for RC beam with haunch retrofitted by CFRP covering PCM Shotcrete. *Proc. Jpn. Concr. Inst.* **2014**, *36*, 1261–1266.
38. Nakamura, S.; Hino, S.; Yamaguchi, K.; Sato, M. Experimental study on seismic strengthening of existing RC bridge pier by PCM shotcrete method. *Proc. Jpn. Concr. Inst.* **2008**, *30*, 1171–1176.

39. Guo, R.; Yamaguchi, K.; Hino, S. Shearing capacity for RC beam with CFRP grid by reinforcement regions in haunch. *Kozo Kogaku Ronbunshu A.* **2015**, *61*, 725–733.
40. Cheng, S.; Chen, Y.; Wang, K. The study of the acrylate copolymer emulsion containing fluorine. *Acta Polym. Sin.* **2002**, *18*, 560–565.
41. Prasad, R.; Nicole, S.; Akshata, K. Exploiting arene-perfluoroarene interactions for dispersion of carbon black in rubber compounds. *Polymer* **2018**, *148*, 247–258.
42. Prasad, R.; Wenfeng, L.; Yu-Ming, C.; Yu, Z.; Sadhan, C. Syndiotactic Polystyrene-Based Ionogel Membranes for High Temperature Electrochemical Applications. *ACS Appl. Mater. Interfaces* **2017**, *9*, 30933–30942.
43. Cai, S.H.; Tang, L.F. Study on polymer cement mortar in concrete patching. *J. Yangtze River Sci. Res. Inst.* **2007**, *24*, 44–47.
44. Guo, R.; Cai, L.H.; Pan, Y.; Liu, Y.L. Experimental study on bonding behavior of interface between concrete and CFRP grid-PCM. *J. Build. Struct.* **2018**, *39*, 19–27.
45. Liu, Z.Q.; Yue, Q.R.; Chen, X.B. Experimental investigation on the anchorage length of CFRP grids. *Ind. Constr.* **2016**, *46*, 18–22.
46. Liu, Z.Q.; Yue, Q.R.; Li, R. Application of FRP grid material in civil engineering. In Proceedings of the 9th National FRP Applied Academic Exchange Conference on Construction Projects, Chongqing, China, 16–18 May 2015; pp. 102–106.
47. Teng, J.G. New-material hybrid structures. *China Civ. Eng. J.* **2018**, *51*, 1–11.
48. Chen, J.F.; Teng, J.G. Shear capacity of FRP-strengthened RC beams: FRP debonding. *Constr. Build. Mater.* **2003**, *17*, 27–41. [[CrossRef](#)]
49. Lu, X.Z.; Tan, Z.; Ye, L.P. Finite element analysis of debonding at the interface between FRP sheet and concrete. *Eng. Mech.* **2004**, *21*, 45–50.
50. Zheng, Y.Z.; Wang, W.W.; Dai, J.G.; Zhu, Z.F. Experimental study on mechanical performance of reinforced concrete beams shear-strengthened with FRP-UHTCC composite. *J. Build. Struct.* **2019**, *40*, 118–126.
51. Ding, Y.; Chen, X.B.; Chen, W.Y. The Flexural Behavior of Beams Strengthened with FRP grid and ECC. In Proceedings of the 5th International Conference on FRP Composites in Civil Engineering, Beijing, China, 27–29 September 2010.
52. Spadea, G.; Bencardino, F.; Sorrenti, F. Structural effectiveness of FRP materials in strengthening RC beams. *Eng. Struct.* **2015**, *99*, 631–641. [[CrossRef](#)]
53. Ferreira, D.; Oller, E.; Barris, C. Shear strain influence in the service response of FRP reinforced concrete beams. *Compos. Struct.* **2015**, *121*, 142–153. [[CrossRef](#)]
54. Li, S.H.; Zhao, G.F.; Wang, S.G. Shear design methodology for RC beams strengthened in shear with CFRP. *China Civ. Eng. J.* **2005**, *51*, 75–80.
55. Chen, G.M.; Teng, J.G.; Asce, M. Shear Strength Model for FRP-Strengthened RC Beams with Adverse FRP-Steel Interaction. *J. Compos. Constr.* **2013**, *17*, 50–66. [[CrossRef](#)]
56. Tan, Z.; Ye, L.P. Experimental research on shear capacity of RC beam strengthened with externally bonded FRP sheets. *China Civ. Eng. J.* **2003**, *36*, 12–18.
57. Schumann, A.; Zobel, R.; Curbach, M. Finite element research of reinforced concrete structures strengthened with textile reinforced concrete (TRC). In Proceedings of the Conference on Computational Modelling of Concrete and Concrete Structures (Euro-C 2018), Bad Hofgastein, Austria, 26 February–1 March 2018.
58. China Association for Engineering Construction Standardization. *Code for Design of Concrete Structures, GB 50010-2010*; China Architecture & Building Press: Beijing, China, 2010; pp. 19–107.
59. Ministry of Housing and Urban-Rural Development of the People’s Republic of China. *Standard for Test Method of Basic Performance on Building Mortar, Shaanxi Architectural Research/Design Institute*; China Architecture & Building Press China: Beijing, China, 2009; pp. 2–18.
60. Ministry of Housing and Urban-Rural Development of the People’s Republic of China. *Standard for Test Method of Mechanical Properties on Ordinary Concrete, GB/T 50081-2002*; China Architecture & Building Press: Beijing, China, 2002; pp. 4–21.
61. Ministry of Housing and Urban-Rural Development of the People’s Republic of China. *Metallic Materials-Tensile Testing at Ambient Temperature, GB/T 228-2002*; China Architecture & Building Press: Beijing, China, 2002; pp. 1–15.

62. Ministry of Housing and Urban-Rural Development of the People's Republic of China. *Standard for Test Method of Concrete Structures, GB/T 50152-2012*; China Architecture & Building Press: Beijing, China, 2012; pp. 11–56.
63. Li, W.W.; Leung, C.K.Y. Effect of shear span-depth ratio on mechanical performance of RC beams strengthened in shear with U-wrapping FRP strips. *Compos. Struct.* **2017**, *177*, 141–157. [[CrossRef](#)]
64. Guo, R.; Pan, Y.; Cai, L.H.; Hino, S. Bonding Behavior of CFRP grid-concrete with PCM shotcrete. *Eng. Struct.* **2018**, *168*, 333–345. [[CrossRef](#)]
65. Wang, B.; Kimitaka, U.; Wu, T.; Dai, H.J.; Guo, R. Experimental investigation of stress transfer and failure mechanism between existing concrete and CFRP grid-sprayed PCM. *Constr. Build. Mater.* **2019**, *215*, 43–58. [[CrossRef](#)]
66. Miyano, N.; Yamaguchi, K.; Taniguchi, K. Shearing capacity for RC beam retrofitted by CFRP covering PCM Shotcrete. *Proc. Jpn. Concr. Inst.* **2013**, *35*, 1423–1428.
67. Japan Road Association. *Specifications for Highway Bridges, Part V Seismic Design*; Japan Road Association: Tokyo, Japan, 2002.
68. Li, W.W.; Leung, C.K. Shear span-depth ratio effect on behavior of RC beam shear strengthened with full-wrapping FRP strip. *J. Compos. Constr.* **2015**, *67*, 1–14. [[CrossRef](#)]
69. Pellegrino, C.; Vasic, M. Assessment of design procedures for the use of externally bonded FRP composites in shear strengthening of reinforced concrete beams. *Compos. Part B Eng.* **2013**, *45*, 727–741. [[CrossRef](#)]
70. Japan Society of Civil Engineers (JSCE). *Concrete Library 88: Design and Construction Guidelines for Concrete Structures Using Continuous Fiber Reinforcement*; Japan Society of Civil Engineers (JSCE): Tokyo, Japan, 1996.
71. Wang, W.W.; Zheng, Y.Z. Experimental research on shear capacity of concrete beams strengthened with BFRP Grid reinforced ECC. In Proceedings of the 9th National FRP Applied Academic Exchange Conference on Construction Projects, Chongqing, China, 29 November–2 December 2015.



© 2019 by the authors. Licensee MDPI, Basel, Switzerland. This article is an open access article distributed under the terms and conditions of the Creative Commons Attribution (CC BY) license (<http://creativecommons.org/licenses/by/4.0/>).